Mechanics of quantum and Sharvin conductors

Jason N. Armstrong, Susan Z. Hua, and Harsh Deep Chopra[*]

Laboratory for Quantum Devices, Materials Program, Mechanical and Aerospace Engineering Department,
The State University of New York at Buffalo, Buffalo, New York 14260, USA

Previously, the authors reported direct evidence of channel saturation and conductance quantization in atomic-sized gold constrictions through mechanical perturbation studies, and also showed that peaks in conductance histograms are insufficient in evaluating their mechanical stability [Armstrong *et al.*, Phys. Rev. B **82**, 195416 (2010)]. In the present study, gold constrictions spanning the range from quantum to semiclassical (Sharvin) conductance regimes are mechanically probed with picolevel resolution in applied force and deformation, along with simultaneous measurements of conductance. While reconfiguration from one constriction size to another is known to occur by apparently random discrete atomic displacements, results reveal a remarkable simplicity—the magnitude of discrete atomic displacements is limited to a small set of values that correspond to elementary slip distances in gold rather than Au-Au interatomic distance. Combined with measurements of the spring constant of constrictions, results reveal two fundamental crossovers in deformation modes with increasing contact diameter—first, from homogeneous shear to defect-mediated deformation at a diameter that is in close agreement with previous predictions [Sørensen *et al.*, Phys. Rev. B **57**, 3283 (1998)]; and second, the discovery of another crossover marking surface- to volume-dominated deformation. A remarkable modulus enhancement is observed when the size of the constrictions approaches the Fermi wavelength of the electrons, and in the limit of a single-atom constriction it is at least two times that for bulk gold. Results provide atomistic insight into the stability of these constrictions and an evolutionary trace of deformation modes, beginning with a single-atom contact.

I. INTRODUCTION

The physical properties of electronic devices composed of a single atom or a few atoms or molecules deviate from their bulk counterparts, requiring semiclassical and ultimately a quantum-mechanical framework for their description. Investigation of these devices provides information on either the extent to which these deviations occur or entirely new phenomena at progressively smaller length scales.[1–26] In particular, as the size of the conductor decreases, the conductance regime changes from classical, to semiclassical (Sharvin), to quantum. At the same time, the effect of atomic discreteness becomes ever more discernible in the experiments. For example, atomic reconfigurations within the conductor cause stepwise changes in conductance. These discrete changes in conductance are not to be confused with conductance quantization; simultaneous measurements of conductance and force on gold constrictions show that the stepwise changes in conductance occur lockstep with stepwise changes in the measured force, signaling the occurrence of atomic rearrangement within the conductor.[20,21,27–37] Given that these atomic-scale devices are acutely sensitive to minute perturbations (electrical, thermal, magnetic, chemical, mechanical, etc.), a fundamental understanding is needed of their mechanical stability, the forces holding them together, and the ability to measure them.[20,21,27,31,33–52]

In particular, through the earliest experimental work of Agraït and co-workers,[31,35] simultaneous measurements of conductance and force in gold constrictions show that a stepwise change in conductance is accompanied by a stepwise change in force, indicating a concomitant atomic rearrangement within the constriction. Theoretical results and simulations by Dreher *et al.*,[21] Hasmy,[53] Todorov and Sutton,[29,30] and Sørensen *et al.*[32] reveal the mechanistic understanding of atomistic processes occurring within the atomic-sized constrictions. Their work reveals correlations between structure and conductance and makes insightful predictions, highlighting the importance of understanding the behavior of atomic-sized samples and leading to the present study.

In a recent study, the authors used picometer-level mechanical perturbations to show direct evidence of channel saturation and conductance quantization in atomic-sized gold constrictions.[20] These results also explained the origin of peaks in conductance histograms and showed that peaks are insufficient in evaluating the mechanical stability of atomic configurations. It was shown that there exists a quasicontinuous distribution of atomic configurations, each with a slightly different conductance. Mechanical stability of these atomic configurations requires knowledge of their spring-constant and deformation characteristics; this information cannot be obtained from conductance histograms. In the present study, the dependence of the spring constant on the constriction size was measured and used to derive the modulus. Results show a remarkable modulus enhancement as the size of the constrictions approaches the Fermi wavelength of the electrons, and in the limit of a single-atom constriction, the enhancement is at least two times that for bulk gold. Furthermore, the magnitude of discrete atomic displacements occurring during reconfiguration from one constriction size to another is measured. Even though there are virtually countless ways in which constrictions may transition from one atomic configuration to another, results reveal a remarkable simplicity—the discrete atomic displacements always occur in units of elementary slip distances for gold. Results reveal two fundamental crossovers in deformation modes with increasing contact diameter, the first one from homogeneous shear to defect-mediated deformation and the second from surface- to volume-dominated deformation.

II. EXPERIMENTAL DETAILS

Gold films (200 nm thick) were magnetron sputtered on silicon substrates in an Ar partial pressure of 3 mtorr in a UHV chamber whose base pressure was $\sim 10^{-8}$–10^{-9} torr. The Au sputtering target was 99.999% pure. Atomic force microscope (AFM) silicon cantilever tips were sputter-coated with Au films (60 nm thick) for force-deformation measurements. During deposition, the cantilevers were periodically rotated relative to the sputtering gun to enhance the uniformity of the gold coating.

A modified AFM (Ambios Q-Scope Nomad) was used for simultaneous measurements of conductance and force-deformation at room temperature in an inert atmosphere. The AFM assembly consisted of a dual piezo configuration, one for coarse and another for fine alignment of the substrate relative to the cantilever tip. With this configuration, the minimum step size was 4 pm and the noise was ~ 5 pm. A range of cantilever spring constants was used (20–70 N/m) to determine the spring constant of various sized constrictions (the need for using cantilevers with different stiffness is discussed later). The cantilevers were precisely calibrated using reference cantilevers available from Veeco Probes (Force Calibration Cantilevers CLFC-NOBO). The photodetector was calibrated using the well-established optical deflection

technique. Conductance traces were recorded at a bias voltage of 250 mV. For all experiments, the piezo was extended or retracted at a rate of 5 nm/s. The experimental setup is described in further detail elsewhere.[20]

III. RESULTS AND DISCUSSION

Figures 1(a)–1(c) show typical examples of simultaneously measured force and conductance traces during the deformation of the constrictions. Their size spans the conductance regimes from being quantized in single-atom to few-atom contacts [inset of Fig. 1(a)] to semiclassical in Figs. 1(a)–1(c). The example traces in Figs. 1(a)–1(c) are obtained by elongating the piezo, which in turn causes the gold-coated AFM tip to push against the gold film to form progressively larger contacts. Figure 1(d) shows an example in which an initially large constriction is progressively broken down to a single atom through piezo retraction. Notice that regardless of the conductance regime, in general each atomic reconfiguration causes a stepwise change in force *and* a stepwise change in conductance. However, occasionally no observable change in conductance is observed corresponding to a stepwise change in force. This is shown in a trace in the inset of Fig. 1(b). It shows that an atomic reconfiguration has occurred in the *vicin-*
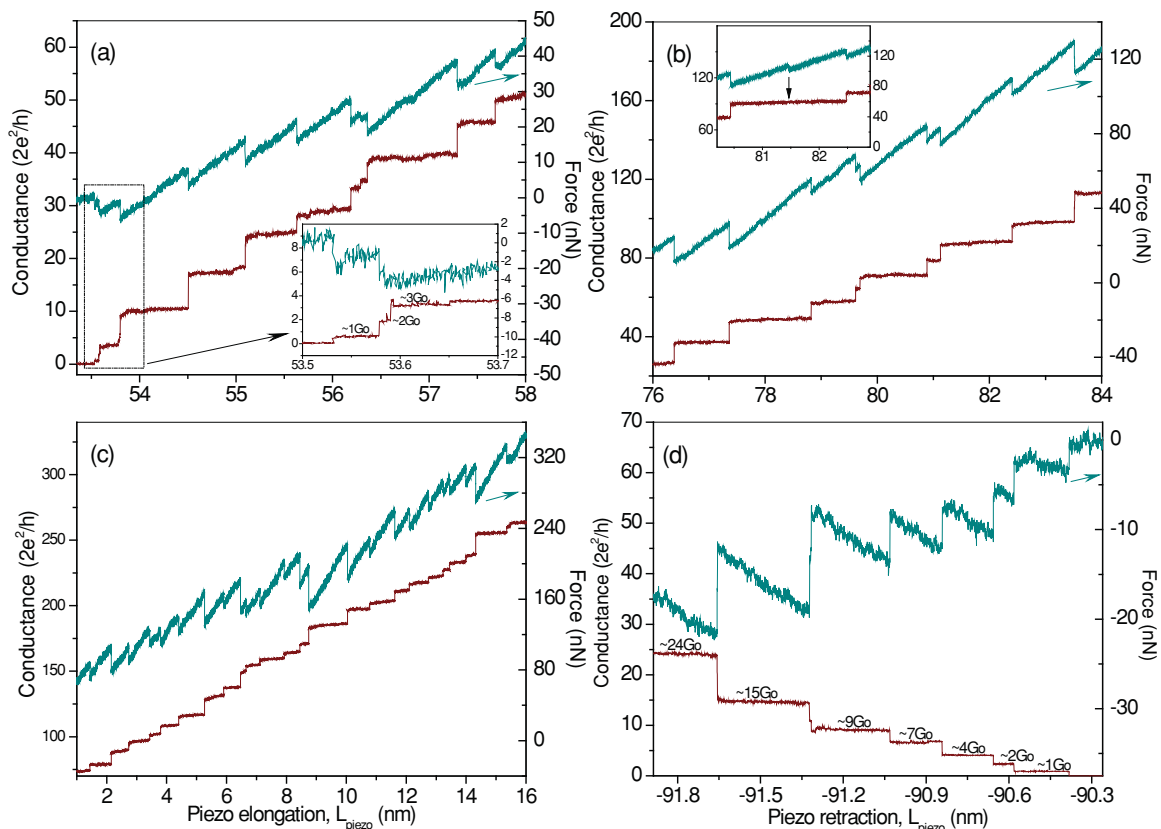

FIG. 1. (Color online) Simultaneously measured conductance and force vs the deformation of the constrictions in different conductance regimes. (a)–(c) corresponds to piezo elongation, which causes the Au-coated AFM tip to push against the Au film to form progressively larger constrictions. The inset in (a) shows the zoom-in view of measured conductance and force in the regime of quantized conductance. Inset in (b) shows a trace that exhibits no observable change in conductance corresponding to a stepwise change in force. Part (d) corresponds to piezo retraction that causes an initially large constrictions to be pulled apart to progressively smaller sizes. The piezo elongation or retraction speed is 5 nm/s.

ity of the constriction without altering the cross-section area of the conductor. This behavior has previously been predicted by simulation studies.[32] This has implications related to the effective length of the constriction, which is discussed in detail later.

After reviewing over a thousand traces, it is estimated that observation of a force jump without a corresponding jump in conductance [inset of Fig. 1(b)] occurs ~1% of the time. Additional examples of this are shown in Figs. S1(a–d) of the supplementary material.[54] Looking into the reverse, namely, observation of a jump in conductance without a corresponding jump in force, it is found that this also occurs ~1% of the time. Examples of this are shown in Figs. S2(a–d) of the supplementary material.[54] One mechanism responsible for this occurrence is the possibility that an atom may have thermally migrated to the constriction, which would change conductance but would not result in a discrete change in force. Low-temperature measurements are currently being initiated, but they are beyond the scope of the present study. Also, notice that unlike bulk materials in which load-deformation curves are separated into an initially elastic region followed by permanent deformation, on the atomic scale the deformation is marked by successive elastic regions separated by catastrophic events during which sudden atomic reconfigurations occur.

Figures 2 and 3 explain various quantities of interest that can be derived from such traces. To explain, Fig. 2(a) schematically shows a gold constriction between a gold-coated cantilever tip and a gold film; the size of the constriction is shown greatly exaggerated relative to the cantilever and the film. As the piezo elongates (defined by its position L_{piezo}), the force on the constriction increases [reflected in the greater deflection of the cantilever for the constriction labeled "A" in Fig. 2(a)]. At some critical force F_1, an atomic reconfiguration occurs to form a new constriction [labeled "Constriction-B" in Fig. 2(a)], and the force drops abruptly from F_1 to F_2. An example of stepwise change in force $\delta F (= F_2 - F_1)$ accompanying an atomic reconfiguration is shown in Fig. 2(b), corresponding to the trace shown in Fig. 1(a). Also accompanying this atomic reconfiguration is a discrete change in length for the constriction $\delta \zeta_{contact}$ and a stepwise change in conductance δG, as shown in Fig. 2(c). Note that the contact deformation ζ in Fig. 2(c) can be directly obtained from the relationship $\zeta = L_{piezo} - L_{cantilever}$; at the instant of an atomic reconfiguration (~10^{13} Hz) marked by the vertical arrows in Figs. 2(b) and 2(c), $\delta L_{piezo} = 0$ and the discrete change in length of the constriction $\delta \zeta_{contact} = -\delta L_{cantilever}$. The inset in Fig. 2(c) also shows SEM micrographs of various gold-coated AFM tip geometries used in the present study. There are two ways to calculate the spring constant of each constriction. First, since the spring constant of the cantilever can be determined precisely (see experimental details), the spring constant of the constriction can be derived from the relationship $K_{contact} = (K_{cantilever} \times K_{measured})/(K_{cantilever} - K_{measured})$. Here, $K_{measured}$ is the combined response of the cantilever and the constriction, which is obtained from the slope of the force versus piezo elongation (or retraction) trace for each constriction, as shown in Fig. 2(b). A range of cantilever spring constants was used (20–70 N/m) to determine the spring constant of various sized constrictions. This is necessitated by the fact that in the limit of $K_{measured} \rightarrow K_{cantilever}$, a small error in $K_{measured}$
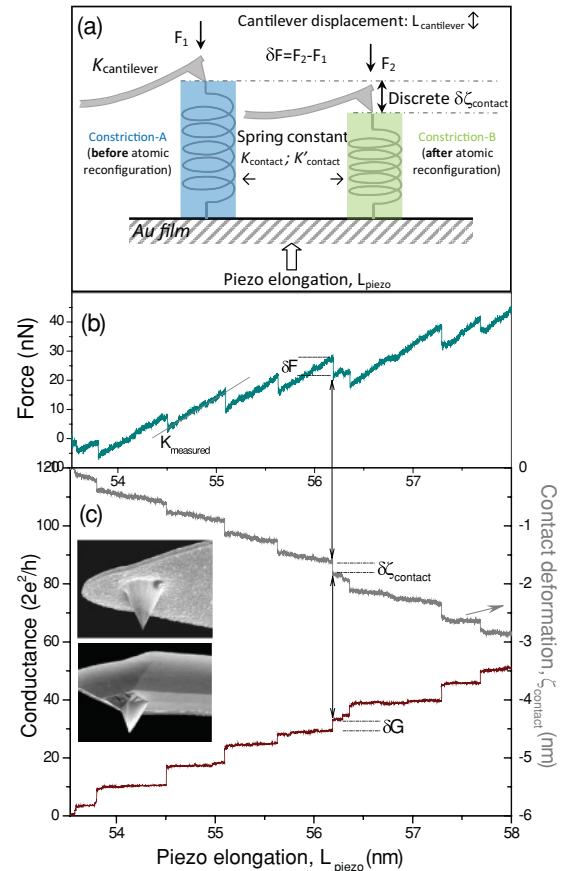

FIG. 2. (Color online) (a) Schematic showing a gold constriction between a gold-coated cantilever tip and a gold film. The size of the constriction is exaggerated relative to the cantilever and the film. (b) and (c) Continuous and discrete changes in force, conductance, and length of various sized constrictions as they assume different atomic configurations. See text for explanation. The inset in (c) shows SEM micrographs of various Au-coated cantilever geometries.
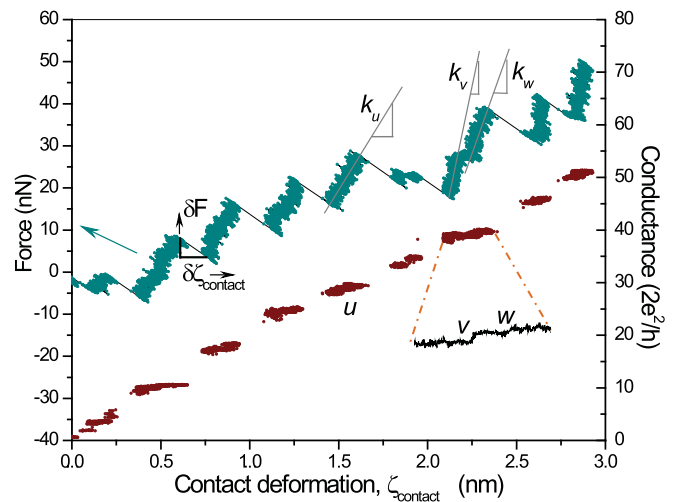

FIG. 3. (Color online) The force on the constrictions as a function of contact deformation $\zeta_{contact}$, whose slopes equals the spring constant of various atomic configurations. The abrupt change in force δF and the accompanying abrupt change in contact length $\delta \zeta_{contact}$ are also labeled.

can lead to a large uncertainty in determining $K_{contact}$. This is shown in the supplementary material (Fig. S3) using the example of $K_{cantilever}$ equal to 24 N/m.[54] An alternate (and equivalent) route to measure the spring constant of individual constrictions is to use traces such as those shown in Figs. 2(b) and 2(c), and replot the force on the constrictions as a function of contact deformation $\zeta_{contact}$, whose slopes then directly provide the spring constant of various atomic configurations. This is shown in Fig. 3 to highlight that the spring constant of various atomic configurations may have different values (for example, K_u, K_v, K_w, etc.). Even two closely spaced configurations, such as those labeled v and w in Fig. 3, may have different spring constants. In Fig. 3, the abrupt change in force δF and the accompanying abrupt change in contact length $\delta\zeta_{contact}$ during atomic reconfiguration are also labeled. The perceptible slope of conductance plateaus represents a small but finite change in conductance within the elastic limits of various atomic configurations; a detailed investigation of strain dependence of conductance for quantum conductors is discussed elsewhere.[20] In the present study, both approaches to calculate the spring constants were used, and they gave similar results (although the former is less cumbersome).

First, consider the magnitudes of discrete atomic displacements during atomic reconfigurations. From hundreds of traces such as the one shown in Fig. 2(c), Fig. 4 plots $\delta\zeta_{contact}$ versus the conductance of the constriction; the inset in Fig. 4 shows a zoom-in view of the plot at lower values of G_o. Figure 4 is obtained by plotting the values of $\delta\zeta_{contact}$ that various constrictions assume upon undergoing atomic reconfiguration. For example, with reference to Fig. 2(c), where the conductance jumps from an initial value of $29G_o$ to $33\,G_o$ [marked by the vertical arrow in Fig. 2(c)], the constriction is seen to undergo a discrete change in length equal to 0.198 nm; Fig. 4 plots this value of $\delta\zeta_{contact}$ at $33\,G_o$. There are several interesting features of this plot. First, the plot is clearly characterized by permissible and prohibited bands of $\delta\zeta_{contact}$; the average permissible values of $\langle\delta\zeta\rangle$ are indicated by the horizontal lines. As opposed to being multiples of the Au-Au bond length of 0.288 nm, all the permissible values of $\langle\delta\zeta\rangle$ represent elementary slip distances (or multiples thereof) on the {111} close-packed planes, with

FIG. 4. (Color online) Plot of $\delta\zeta_{contact}$ vs the conductance of the constrictions formed by piezo elongation; the inset shows a zoom-in view at lower values of G_o. See text for an explanation.

the constriction axis along the $\langle110\rangle$, $\langle111\rangle$, or $\langle100\rangle$ directions. The present study reveals the existence of various levels due to picometer resolution in measured displacements, whereas previously, only a single band centered at an average value of 0.152 nm was reported for compression.[34] Notice the four sharply separated permissible $\langle\delta\zeta\rangle$ levels in the inset of Fig. 4. The distances of 0.049, 0.079, and 0.088 nm correspond to hcp→fcc slip distances on {111} planes with the constriction axis along the [110], [111], and [100] directions, respectively; the value of 0.098 nm corresponds to fcc→hcp slip distance with the constriction axis along the [110] direction; see Ref. 34 for crystallography related to these values for gold. Figure 4 shows that these four sharply defined levels transition into a diffuse band with an average value of ~0.168 nm, and this crossover occurs at a conductance value of $19\,G_o$. The diameter corresponding to this conductance value is equal to 1.45 nm (using the Sharvin formula, discussed later). Even though this value is for the case of pushing the cantilever into the gold film, this crossover diameter agrees remarkably well with the theoretically predicted constriction diameter of 1.5 ± 0.3 nm for crossover from homogeneous shear to defect-mediated deformation for gold in tension.[32] The defect-mediated deformation causes the sharply defined discrete displacement levels to form a diffuse band. Also, the average value of $\langle\delta\zeta\rangle$ for this band is close to the elementary slip distance of 0.166 nm on the {111} planes along the $\langle112\rangle$ direction in gold, which further confirms dislocation-mediated deformation. In Fig. 4, as the size of the constrictions becomes larger, there is a higher probability for simultaneous slip on {111} planes. This explains the existence of the 0.504 nm band, which is three times $\langle\delta\zeta\rangle$ equal to 0.168 nm; however, the absence of another band at twice the value of 0.168 nm is interesting and needs to be studied further. Also, notice that the band at 0.393 nm is four times $\langle\delta\zeta\rangle$ equal to 0.098 nm, and lies in the size regime in which crossover from surface- to volume-dominated deformation occurs, as discussed below.

Next, consider the vertical arrows, labeled I($7\,G_o$), II($19\,G_o$), III($37\,G_o$), and V($100\,G_o$) in Fig. 4; the absence of an arrow labeled "IV" is explained in the following. These arrows mark a threshold conductance value above which a new level of $\langle\delta\zeta\rangle$ becomes permissible. For example, constrictions whose size is greater than $37\,G_o$ (marked by arrow III) may undergo a discrete change in length at a new value of $\langle\delta\zeta\rangle$ equal to 0.393 nm *in addition to* the permissible values of $\langle\delta\zeta\rangle$ that are available to them below $37\,G_o$. The conductance values in the parentheses adjacent to the arrows have special significance. As shown schematically in Fig. 4, a value of $7\,G_o$ corresponds to the formation of a complete ring of gold atoms around a single atom for a total of seven atoms; the conductance of a single atom of gold saturates at $1\,G_o$.[20,22] Similarly, values of $19\,G_o$ and $37\,G_o$ represent the completion of the second and the third rings around the gold atom, corresponding to 19 and 37 atoms, respectively. While the fourth ring (61 atoms) is expected to appear at $61\,G_o$, it is missing in Fig. 4, whereas the fifth ring with a total of 91 atoms appears experimentally at ~$100\,G_o$, as marked by arrow V. As shown in the following, the missing fourth ring lies in between the crossover from surface- to volume-dominated deformation behavior, and this transition region is demarcated in Fig. 4. Note that the number of channels in an atom is equal
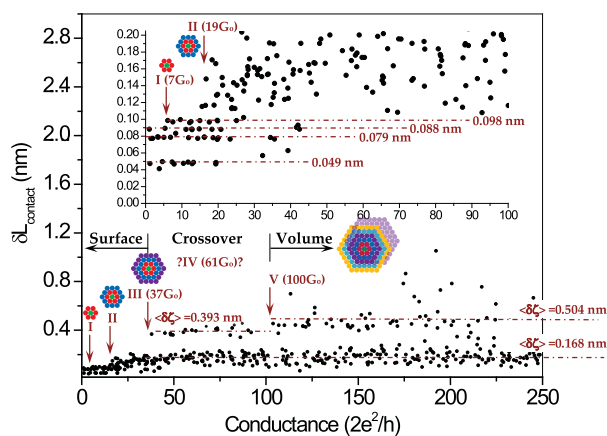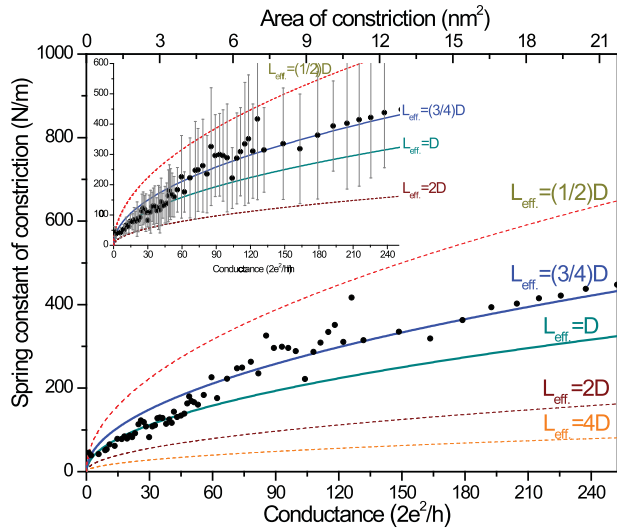
FIG. 5. (Color online) (a) Spring constants K_{contact} of the constrictions as a function of their conductance and also their area calculated using Sharvin's semiclassical formula. The contacts are formed by piezo elongation. Each data point represents an average over 20 measurements; the inset shows their standard deviation. For contacts with conductance less than $10\,G_o$, each point is an average over three measurements. The solid and dotted lines are theoretical values of the spring constant for different L_{eff}/D ratios, using a modulus of 78.5 GPa for bulk gold and derived using Sharvin formula.
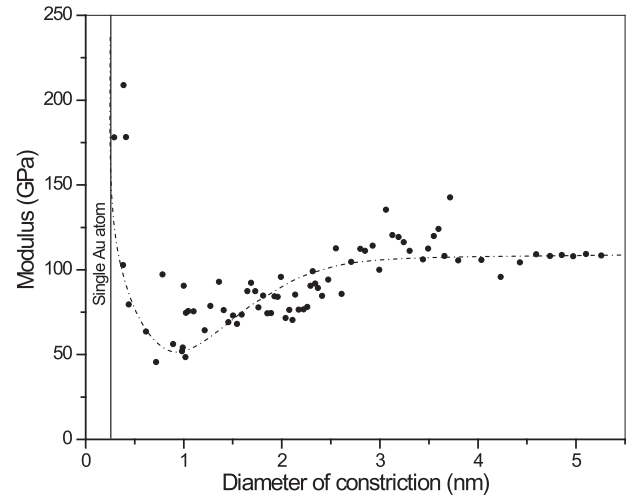

FIG. 6. The size dependence of the modulus of the constrictions assuming $L_{\text{eff}} = D$. The dotted line is an aid to the eyes.

to its valence electrons.[22] Thus for gold, one atom can have a maximum of $1\,G_o$ of conductance. Figure 4 schematically shows rings of atoms around a single gold atom for various crossovers only as an idealization. Note that at III, number of atoms on the surface is ~50%.

Figure 5 plots the spring constant K_{contact} as a function of conductance (lower abscissa) and area (upper abscissa) of the constriction. In Fig. 5, the solid and dotted lines are theoretical values of the spring constant ($K = EA/L$) based on a modulus E of 78.5 GPa for bulk gold and derived using the Sharvin formula for different ratios L_{eff}/D of length to the diameter of the constrictions.[55,56] The Sharvin formula relates the conductance G_s to the area A of the constriction by the relationship $G_s = (2e^2/h)(\pi A/\lambda_F^2) = G_o(\pi A/\lambda_F^2)$; here, $(2e^2/h) = G_o$ is the quantum of conductance, e is the quantum of charge, h is Planck's constant, and λ_F is the Fermi wavelength ($=0.52$ nm for gold). The Sharvin formula allows the area of the constriction to be estimated for a given conductance, as shown on the upper abscissa in Fig. 5 (assuming a circular cross section). However, *a priori*, the effective length L_{eff} of the constrictions is not known, and the solid and dotted lines plot the spring constants assuming different ratios of length to the diameter. Figure 5 clearly shows that up to a certain size of the constriction, the experimentally measured data points closely follow the trend line represented by $L_{\text{eff}} = D$ and then transition to the trend line for $L_{\text{eff}} = (3/4)D$ for larger constrictions. This crossover can be seen to occur at conductance values between $\sim47\,G_o$ and $67\,G_o$, corresponding to constriction cross-section areas between ~4.1 and 5.7 nm^2 (or a constriction diameter of 2.27–2.67 nm). This crossover region corresponds well with the crossover region shown in Fig. 4.

Recall that in Fig. 5, the theoretical trend lines for spring constants for various L_{eff}/D ratios were plotted by assuming the modulus value for bulk gold. Conversely, one can arbitrarily assume a ratio for L_{eff}/D to assess the size dependence of the modulus. Figure 6 plots the size dependence of the modulus by assuming $L_{\text{eff}} = D$. The significance of assuming $L_{\text{eff}} = D$ is that it represents the limiting case of a single-atom contact, where the diameter of the atom equals its length. Figure 6 shows that there is a large modulus enhancement up to two times the value for bulk gold in the limit of a single-atom constriction. As the diameter of the constriction increases, there is a minimum in modulus at a diameter of ~1.0 nm, corresponding to a constriction area ~0.78 nm^2 and a conductance of $\sim9\,G_o$. With a further increase in the size of the constriction, the modulus approaches the bulk value. This occurs at a constriction diameter of ~2.7 nm, corresponding to the conductance of $\sim67\,G_o$. It is consistent with the missing transition for $\langle\delta\zeta\rangle$ at $61\,G_o$ in Fig. 4 for the fourth gold ring, corresponding to the crossover from surface- to volume-dominated deformation.

Figure 7 plots $\delta\zeta_{\text{contact}}$ versus conductance for the case of initially large constrictions being pulled apart to progressively smaller sizes through piezo retraction; see, for example, the trace in Fig. 1(d). In contrast to Fig. 4, where constrictions were pushed into progressively larger diameters through piezo elongation, the permissible and prohibited bands of $\delta\zeta_{\text{contact}}$ in Fig. 7 are less well defined; this difference arises simply because of the fact that in the former case, the constriction's neck cannot be stretched, whereas in pulling, a constriction has the possibility to elongate without changing its effective cross-section area (which determines its conductance). Consequently, a range of L_{eff}/D ratios may be expected for piezo retraction, as shown in the following. Another salient feature of Fig. 7 is the absence of any level for $\delta\zeta_{\text{contact}}$ below 0.098 nm. By comparison, the inset in Fig. 4 shows three well-defined levels below 0.098 nm. However, threshold conductance values above which a new level of $\langle\delta\zeta\rangle$ becomes permissible can still be roughly seen, as marked by the vertical arrows. Figure 8(a) plots the spring constant as a function of size for this data set. The zoom-in view in the inset of Fig. 8(a)
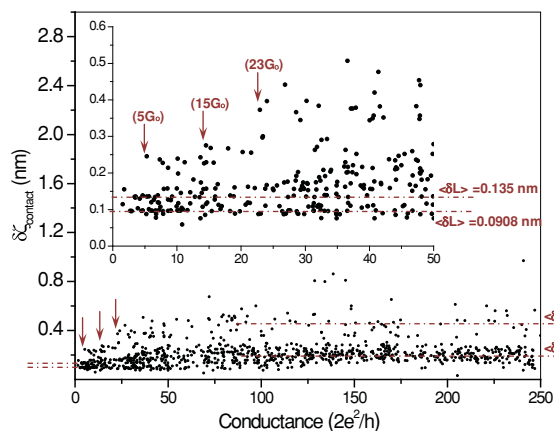
FIG. 7. (Color online) Plot of $\delta\zeta_{contact}$ vs the conductance of the constrictions formed by piezo retraction; the inset shows a zoom-in view at lower values of G_o. See text for explanation.

shows that only in the limit of single-atom constriction (marked by the vertical arrow at $1G_o$) do the experimental spring constant values fall on the $L_{eff} = D$ trend line. This is followed by a transition to the trend line for $L_{eff} = 2D$ for constrictions up to $\sim 5\,G_o$ (as marked by the vertical arrow), beyond which the spring constants follow a range of L_{eff}/D ratios. In contrast to the data in Fig. 5, where the spring constant data transition to a *lower* L_{eff}/D ratio within a well-defined transition region, the data in Fig. 8(a) trend toward *higher* L_{eff}/D ratios of up to 6–8 for larger-sized constrictions. Analogous to the procedure described in Fig. 6, the size dependence of the modulus is plotted in Fig. 8(b). Again, the salient feature of this plot is the *apparently* large enhancement in modulus in the limit of a single atom that is up to five times that of the modulus for bulk gold. However, the modulus is calculated by assuming $L_{eff} = 6D$. If one were to take another ratio for L_{eff}/D (say, $L_{eff} = D$), the calculated values of the modulus in the limit of a single atom would be much smaller. Therefore the validity of modulus enhancement has to be ascertained, and the following approach provides a benchmark for validating its existence.

Figures 9(a) and 9(b), respectively, map L_{eff}/D ratios as a function of contact diameter using the spring-constant data shown in Fig. 5 (for the case of constrictions formed by piezo elongation) and Fig. 8(a) (for the case of piezo retraction), assuming the modulus value for bulk gold. Figure 9(a) shows that in the limit of a single atom, the L_{eff}/D actually becomes less than 1 (shown encircled). This is physically impossible, as $L_{eff} = D$ is the smallest possible value that a single-atom constriction can take. This shows that the modulus enhancement indeed exists and is at least two times the value in the bulk (the lower bound). On the other hand, the data in Fig. 9(b) might suggest the absence of any modulus enhancement, since the value of the L_{eff}/D ratio does not drop below 1 in the limit of a single-atom constriction (shown encircled). However, in describing the L_{eff}/D ratio, L_{eff} is the effective length over which the deformation occurs, as shown schematically in Fig. 9(b). Thus, for example at $L_{eff}/D = 1$, the definition implies that the deformation only occurs over a length equal to the diameter of the constriction, and would have no impact beyond that. This is obviously unrealistic, and in the limit of a single atom, the deformation surely extends
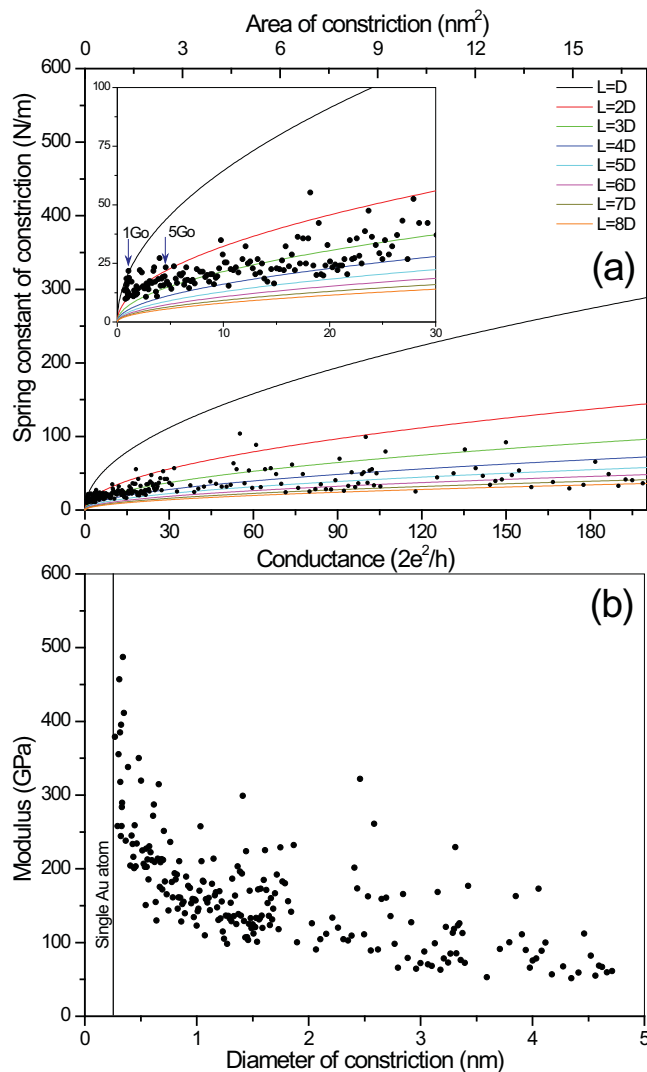

FIG. 8. (Color online) (a) Spring constant $K_{contact}$ of the constrictions as a function of their conductance and also their area calculated using Sharvin formula. The contacts are formed by piezo retraction. Each data point represents an average over 25 measurements; for contacts with conductance less than $10\,G_o$, each point is an average over three measurements. The inset shows the zoom-in view at lower values of conductance, which shows L_{eff}/D ratio of 1 in the limit of single-atom contact, increasing to 2 for conductance up to $5\,G_o$, and then taking a range of higher ratios for larger sized constrictions. The solid and dotted lines are theoretical values of the spring constant for different L_{eff}/D ratios, using a modulus of 78.5 GPa for bulk gold and derived using Sharvin formula. (b) The size dependence of the modulus of the constrictions assuming $L_{eff}/6D$.

beyond one atomic diameter.[32] As shown earlier with the aid of an example trace in the inset of Fig. 1(b), forces can cause an atomic reconfiguration away from the constriction. Although the compression data in Fig. 9(a) clearly show that the lower bound of modulus enhancement is at least two times that for bulk gold, without precise information on contact geometry and deformation away from the constriction for Fig. 9(b), it is not possible to ascertain the upper bound of this enhancement.

Previous studies based on density-functional theory and dynamic simulations predict bond strengthening at a comparable scale, which is seen from modulus enhancement in the present
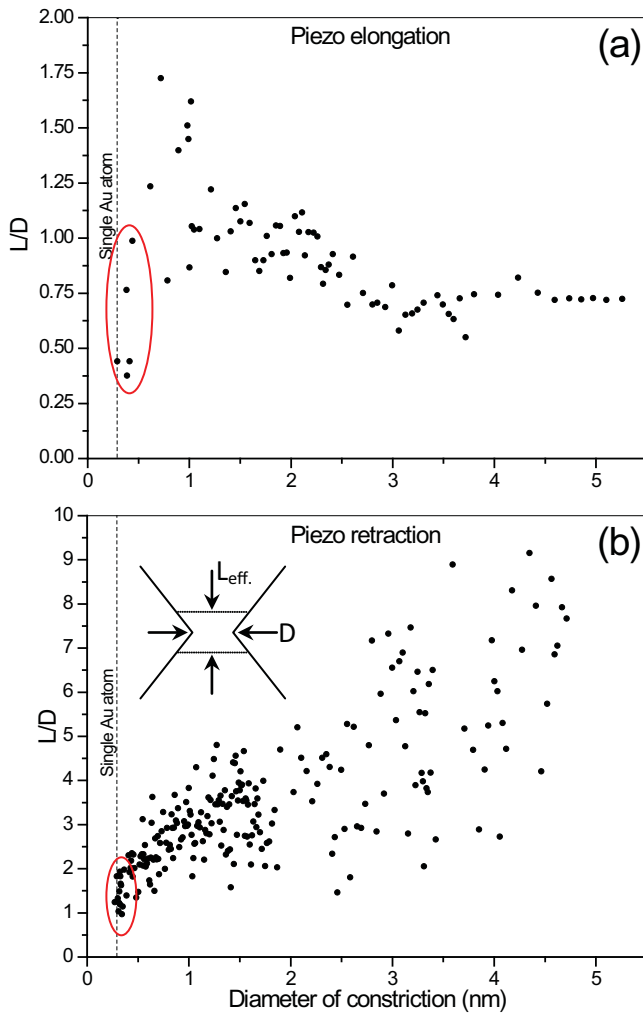
FIG. 9. (Color online) (a) Map of L_{eff}/D ratio as a function of contact diameter using the spring constants shown in Fig. 5 for the case of constrictions formed by piezo elongation, and (b) for the case of piezo retraction in Fig. 8(a), assuming modulus value of bulk gold.

the spring constant gets measured over different orientations of atomic configurations and saturates at ~100 GPa for large diameters. This value is slightly higher than the modulus of polycrystalline gold (~78 GPa) and is close to the modulus of 110 GPa along the ⟨111⟩ direction (the lowest value of the modulus for gold being 40 GPa along the ⟨100⟩ direction). A value of the modulus closer to the ⟨111⟩ direction is also in accord with Hasmy's molecular-dynamics simulations, which predict ⟨111⟩ as the favorable reconstruction.[53] Finally, the definition of the modulus in the context of atomic-sized samples is best seen from the point of view of the slope of the net attractive or repulsive forces versus interatomic distances (as opposed to the classical mechanics definition).

IV. CONCLUSIONS

Results show a remarkable modulus enhancement as the size of the constrictions approaches the Fermi wavelength of the electrons, and in the limit of a single-atom constriction it is at least two times that for bulk gold. The observed modulus enhancement by a factor of 2 represents the lower bound. Precise information on contact geometry and deformation away from the constrictions is needed to establish the upper bound of modulus enhancement.

While reconfiguration from one constriction size to another is known to occur by apparently random discrete atomic displacements, results show that the magnitude of these displacements is not arbitrary but is limited to a small set of values defined by the gold crystallography rather than Au-Au interatomic distance.

Two fundamental crossovers in deformation modes are observed with increasing contact diameter. The first crossover is from homogeneous shear to defect-mediated deformation at a constriction diameter (~1.45 nm) that not only corresponds with the previously predicted value (1.5 ± 0.3 nm) for tension,[32] but is even more sharply demarcated for compression. Another crossover is observed at constriction diameters between 2.0 and 3.2 nm, marking the transition from surface- to volume-dominated deformation.

The results provide atomistic insight into the mechanics of these constrictions and reveal the evolutionary trace of deformation modes, beginning with a single-atom contact. Whether the reversible deformation of individual constrictions follows linear elasticity or nonlinear elasticity remains to be further investigated and is beyond the scope of the present studies.

study.[29,57] As to the extent of modulus enhancement, note that Sharvin analysis deviates in the limit of a single atom, but the estimate one gets provides a conservative rather than an exaggerated estimate of the enhancement. The atomic diameter of a gold atom is known precisely, and using that value, the estimated modulus enhancement from the measured spring constants would be 2.5 times that for bulk gold (instead of two times using the Sharvin estimate). Similarly, using diameter values estimated from single-atom gold chains,[58] a modulus enhancement by a factor of 3 would be obtained. However all the data are base-lined using the Sharvin estimate simply because it gives the most conservative estimate of modulus enhancement. Also, note that over repeated measurements,

*Author to whom all correspondence should be addressed: hchopra@buffalo.edu

[1] N. Oncel, J. Phys. Condens. Matter **20**, 393001 (2008).

[2] A. Calzolari, C. Cavazzoni, and M. Buongiorno-Nardelli, Phys. Rev. Lett. **93**, 096404 (2004).

[3] A. Sperl, J. Kröger, N. Néel, H. Jensen, R. Berndt, A. Franke, and E. Pehlke, Phys. Rev. B **77**, 085422 (2008).

[4] N. Nilius, T. M. Wallis, and W. Ho, Science **297**, 1853 (2002).

[5] J. Lagoute, X. Liu, and S. Fölsch, Phys. Rev. B **74**, 125410 (2006).

[6] K. Schouteden, E. Lijnen, D. A. Muzychenko, A. Ceulemans, L. F. Chibotaru, P. Lievens, and C. Van Haesendonck, Nanotechnology **20**, 395401 (2009).

[7] Y. Selzer and D. L. Allara, Annu. Rev. Phys. Chem. **57**, 593 (2006).

[8] A. Sperl, J. Kröger, and R. Berndt, Phys. Status Solidi B **247**, 1077 (2010).

[9] S. L. Elizondo and J. W. Mintmire, Int. J. Quantum Chem. **105**, 772 (2005).

[10] S. Díaz-Tendero, S. Fölsch, F. E. Olsson, A. G. Borisov, and J.-P. Gauyacq, Nano Lett. **8**, 2712 (2008).

[11] S. N. Behera, S. Gayen, G. V. Ravi Prasad, and S. M. Bose, Physica B **390**, 124 (2007).

[12] H. D. Chopra, M. R. Sullivan, J. N. Armstrong, and S. Z. Hua, Nat. Mater. **4**, 832 (2005).

[13] D. G. Cahill, W. K. Ford, K. E. Goodson, G. D. Mahan, A. Majumdar, H. J. Maris, R. Merlin, and S. R. Phillpot, J. Appl. Phys. **93**, 793 (2003).

[14] S. Díaz-Tendero, A. G. Borisov, and J. P. Gauyacq, Phys. Rev. B **76**, 155428 (2007).

[15] T. Nautiyal, S. J. Youn, and K. S. Kim, Phys. Rev. B **68**, 033407 (2003).

[16] A. van Houselt, N. Oncel, B. Poelsema, and H. J. W. Zandvliet, Nano Lett. **6**, 1439 (2006).

[17] K. Hansen, E. Lægsgaard, I. Stensgaard, and F. Besenbacher, Phys. Rev. B **56**, 2208 (1997).

[18] E. Scheer, P. Joyez, D. Esteve, C. Urbina, and M. H. Devoret, Phys. Rev. Lett. **78**, 3535 (1997).

[19] Y. Kihira, T. Shimada, Y. Matsuo, E. Nakamura, and T. Hasegawa, Nano Lett. **9**, 1442 (2009).

[20] J. N. Armstrong, R. M. Schaub, S. Z. Hua, and H. D. Chopra, Phys. Rev. B **82**, 195416 (2010).

[21] M. Dreher, F. Pauly, J. Heurich, J. C. Cuevas, E. Scheer, and P. Nielaba, Phys. Rev. B **72**, 075435 (2005).

[22] E. Scheer, N. Agrait, J. C. Cuevas, A. L. Yeyati, B. Ludoph, A. Martin-Rodero, G. R. Bollinger, J. M. van Ruitenbeek, and C. Urbina, Nature (London) **394**, 154 (1998).

[23] S. Wippermann, N. Koch, and W. G. Schmidt, Phys. Rev. Lett. **100**, 106802 (2008).

[24] M. Brandbyge, J. Schiotz, M. R. Sorensen, P. Stoltze, K. W. Jacobsen, J. K. Norskov, L. Olesen, E. Laegsgaard, I. Stensgaard, and F. Besenbacher, Phys. Rev. B **52**, 8499 (1995).

[25] A. I. Yanson, G. R. Bollinger, H. E. van den Brom, N. Agrait, and J. M. van Ruitenbeek, Nature (London) **395**, 783 (1998).

[26] H. Ohnishi, Y. Kondo, and K. Takayanagi, Nature (London) **395**, 780 (1998).

[27] U. Landman, W. D. Luedtke, N. A. Burnham, and R. J. Colton, Science **248**, 454 (1990).

[28] A. P. Sutton and J. B. Pethica, J. Phys. Condens. Matter **2**, 5317 (1990).

[29] T. N. Todorov and A. P. Sutton, Phys. Rev. Lett. **70**, 2138 (1993).

[30] T. N. Todorov and A. P. Sutton, Phys. Rev. B **54**, R14234 (1996).

[31] G. Rubio, N. Agraït, and S. Vieira, Phys. Rev. Lett. **76**, 2302 (1996).

[32] M. R. Sørensen, M. Brandbyge, and K. W. Jacobsen, Phys. Rev. B **57**, 3283 (1998).

[33] S. P. Jarvis, M. A. Lantz, H. Ogiso, H. Tokumoto, and U. Durig, Appl. Phys. Lett. **75**, 3132 (1999).

[34] P. E. Marszalek, W. J. Greenleaf, H. Li, A. F. Oberhauser, and J. M. Fernandez, Proc. Nat. Acad. Sci. USA **97**, 6282 (2000).

[35] G. Rubio-Bollinger, S. R. Bahn, N. Agraït, K. W. Jacobsen, and S. Vieira, Phys. Rev. Lett. **87**, 026101 (2001).

[36] M. D. Huntington, J. N. Armstrong, M. R. Sullivan, S. Z. Hua, and H. D. Chopra, Phys. Rev. B **78**, 035442 (2008).

[37] T. Kizuka, Phys. Rev. B **77**, 155401 (2008).

[38] S. Ciraci, E. Tekman, A. Baratoff, and I. P. Batra, Phys. Rev. B **46**, 10411 (1992).

[39] O. Custance, R. Perez, and S. Morita, Nat. Nano. **4**, 803 (2009).

[40] Y. Sugimoto, M. Abe, S. Hirayama, N. Oyabu, O. Custance, and S. Morita, Nat. Mater **4**, 156 (2005).

[41] Y. Sugimoto, P. Pou, O. Custance, P. Jelinek, M. Abe, R. Perez, and S. Morita, Science **322**, 413 (2008).

[42] M. Ternes, C. P. Lutz, C. F. Hirjibehedin, F. J. Giessibl, and A. J. Heinrich, Science **319**, 1066 (2008).

[43] D. M. Eigler and E. K. Schweizer, Nature (London) **344**, 524 (1990).

[44] L. Bartels, G. Meyer, and K. H. Rieder, Phys. Rev. Lett. **79**, 697 (1997).

[45] A. Deshpande, H. Yildirim, A. Kara, D. P. Acharya, J. Vaughn, T. S. Rahman, and S. W. Hla, Phys. Rev. Lett. **98**, 028304 (2007).

[46] S.-W. Hla, K.-F. Braun, and K.-H. Rieder, Phys. Rev. B **67**, 201402 (2003).

[47] L. Gross, F. Mohn, N. Moll, P. Liljeroth, and G. Meyer, Science **325**, 1110 (2009).

[48] X. L. Li, S. Z. Hua, H. D. Chopra, and N. J. Tao, Micro & Nano Lett., IET **1**, 83 (2006).

[49] F. Grill and F. Moresco, J. Phys. Condens. Matter **2006**, S1887 (2006).

[50] F. Moresco, Phys. Rep. **399**, 175 (2004).

[51] J. Kröger, N. Néel, and L. Limot, J. Phys. Condens. Matter **20**, 222301 (2008).

[52] F. Moresco and A. Gourdon, Proc. Natl. Acad. Sci. USA **102**, 8809 (2005).

[53] A. Hasmy and E. Medina, Phys. Rev. Lett. **88**, 096103 (2002).

[54] See supplemental material at [http://link.aps.org/supplemental/10.1103/PhysRevB.83.235422]. Figures S1(a–d) show additional examples of a stepwise change in force without a corresponding stepwise change in conductance. Figures S2(a–d) show examples of a stepwise change in conductance without a corresponding stepwise change in force. Figure S3 shows a graph highlighting that a small error in measured spring constant leads to a large uncertainty in determining the spring constant of the constriction.

[55] Y. V. Sharvin, Zh. Eksp. Teor. Fiz. **48**, 984 (1965) [Sov. Phys. JETP **21**, 655 (1965)].

[56] J. A. Torres, J. I. Pascual, and J. J. Sáenz, Phys. Rev. B **49**, 16581 (1994).

[57] M. Methfessel, D. Hennig, and M. Scheffler, Appl. Phys. A **55**, 442 (1992).

[58] C. Untiedt, A. I. Yanson, R. Grande, G. Rubio-Bollinger, N. Agrait, S. Vieira, and J. M. van Ruitenbeek, Phys. Rev. B **66**, 085418 (2002).